Scatterer Density in Nonlinear Diffusion for Speckle Reduction in Ultrasound Imaging: The Isotropic Case

Ahmed Badawi

Abstract—This paper proposes a method for speckle reduction in medical ultrasound imaging while preserving the edges with the added advantages of adaptive noise filtering and speed. A nonlinear image diffusion method that incorporates local image parameter, namely, scatterer density in addition to gradient, to weight the nonlinear diffusion process, is proposed. The method was tested for the isotropic case with a contrast detail phantom and varieties of clinical ultrasound images, and then compared to linear and some other diffusion enhancement methods. Different diffusion parameters were tested and tuned to best reduce speckle noise and preserve edges. The method showed superior performance measured both quantitatively and qualitatively when incorporating scatterer density into the diffusivity function. The proposed filter can be used as a preprocessing step for ultrasound image enhancement before applying automatic segmentation, automatic volumetric calculations, or 3D ultrasound volume rendering.

Keywords—Ultrasound imaging, Nonlinear isotropic diffusion, Speckle noise, Scattering.

I. INTRODUCTION

MEDICAL ultrasound is a mode of medical imaging that has a wide array of clinical applications, both as a primary modality and as an adjunct to other diagnostic procedures [1]. The clinical utility of ultrasound imaging is in large part due to three characteristics. Ultrasound is a real-time modality, does not utilize ionizing radiation, and provides quantitative measurement and imaging of blood flow. However, an inherent characteristic of ultrasound imaging and any type of coherent imaging in general, is the presence of speckle noise. Speckle is a random interference pattern in an image formed with coherent radiation of a medium containing many sub-resolution scatterers. The texture of the observed speckle pattern does not correspond to underlying structure. Speckle has a negative impact on ultrasound imaging. Bamber and Daft show a reduction of lesion detectability of approximately a factor of eight due to the presence of speckle in the image [2]. This radical reduction in contrast resolution is responsible for the poorer effective resolution of ultrasound compared to X-ray or MRI.

Therefore, the methods of speckle reduction have been established in the past 40 years as one of the active research fields in medical ultrasound information processing [3]. Adaptive filtering for speckle reduction has been studied by Bamber et al. [7] in order to reduce speckles in ultrasound images. Many speckle reduction filters have been developed with different assumption about the speckle model [14, 29], having the multiplicative model the one mostly used, and paving the way for those described by Lee[30], Frost et al. [31], and Kuan et al. [32-33]. Yu and Acton [34] have proposed a filtering scheme based on filters first described by Lee and Frost, called speckle reducing anisotropic diffusion (SRAD). This SRAD filter has shown a very good performance with different levels of speckle. S. Adja-Fernandez and C. Alberola-Lopez [35] derived an anisotropic diffusion filter that does not depend on a linear approximation of the speckle model as in the SRAD case and they focused on the problem of estimation of coefficient of variation of both signal and noise. However, denoising techniques should not only reduce the noise, but do so without blurring or changing the location of the edges. Hence, techniques, based on the use of partial differential equations, have been extensively studied since the early work of Perona and Malik in 1987 [8] and others [9-16]. The idea behind the use of the diffusion equation in image processing arose from the use of the Gaussian filter in multi-scale image analysis. If the diffusivity function is a constant, i.e., independent of image positions (x, y) or time (t), it leads to a linear diffusion equation [8], with a homogeneous diffusivity. In this case, all locations in the image, including the edges are smoothed equally. This is, of course, undesirable, and a simple improvement would be to change diffusivity with the location x and y in the image, thus converting the equation into a linear diffusion equation with non-homogeneous diffusivity. If the diffusivity function is image dependent, then the linear diffusion equation becomes a non-linear diffusion equation [10-16]. For example, by using a function that was based on the derivative of the image at time t, Perona and Malik [9] were able to control the diffusion near the edges in the image. Isotropic non-linear diffusion is the case where the diffusivity is scalar while anisotropic diffusion is the case where the diffusivity function is varying with both the edge location and its directions [10-16, 40].

Ahmed Badawi is a visiting professor with University of Tennessee, Knoxville, Biomedical Engineering Department, 315 Perkins Hall, 1506 Middle Dr., Knoxville, TN, 37996, USA (phone: 865-974-6009; fax: 865-946-1787; e-mail: ambadawi@utk.edu). He is a professor on leave at Systems & Biomedical Engineering Department, Cairo University.

Thus, diffusion across the edge can be prevented while allowing diffusion along the edge. This prevents the edge from being smoothed during the denoising process. There are several factors that must be considered in the use of diffusion-based techniques for denoising. These include the choice of the diffusivity function, setting any parameters used in the diffusivity function [11-14], the method of discretization of the PDE, the options used in the solution of the PDE including the time for which it is evolved, and the method used for solving the linear system of equations. The tensor formulation of nonlinear coherent diffusion method (NCD) was presented in [14] and was implemented in real time. NCD change progressively from isotropic diffusion through anisotropic coherent diffusion to, finally, mean curvature motion according to speckle noise contents and anisotropy. A better quality of diffusion using NCD method was obtained compared to adaptive weighted median filter (AWFM), wavelet shrinkage (WS), and wavelet shrinkage and contrast enhancement (WSCE) methods [14]. While NCD had a better performance compared to AWFM, WS, and WSCE, it has several criticisms mentioned in [40]. One such criticism being anisotropic tensor formulation is regarding the size of speckle that may occupy more than the size of a pixel. A speckle reduction and structure enhancement method by multichannel median boosted anisotropic diffusion was presented in [40] and showed to be superior to methods like AWFM and Gaussian regularized anisotropic diffusion. The method presented in [40] was successful compared to AWFM and Gaussian regularized anisotropic diffusion, their results with test ultrasound phantoms and clinical ultrasound images of different levels of speckle noise, size, and distribution were not compared. Mean square error and signal to noise ratio were used for tuning and evaluating the denoising process [14, 17-18]. Signal-to-noise ratio (SNR) and Peak signal-to-noise-ratio (PSNR) image measures are derived from the root mean squared error (RMSE) and used as an image quality measures in compression, representation, and standards [24, 39]. Higher quality measures do not always mean better visual quality of enhanced edges and denoised structures. The universal image quality index (Q) measures the distortion between two images and model this image distortion as a combination of three factors; loss of correlation, luminance distortion, and contrast distortion [41]. Edge enhancement and edge preserving quantitative evaluation is applied by the Pratt's figure of merit (FOM) [42] as a measure for edge preservation and edge enhancement between ideal image and processed one and can be used as a measure of objects segmentation quality.

Our paper proposes a new ultrasound diffusion enhancement method suitable for processing ultrasound images for speckle reduction with edge enhancement. This method takes into consideration an ultrasound scatterer density in addition to the gradient for weighting the diffusivity function. The resulting diffusion filter combines the advantages of locally adaptive filtering and computational speed using the fast and stable diffusion equation discretization, semi-implicit scheme using additive operator splitting (*AOS*), and coupled with a new automatic criteria to stop the diffusion process with preserving edges, geometry, and visual quality of the image.

The rest of this paper's structure is organized as follows. Section II.A gives a brief introduction to the nonlinear diffusion filtering and its applicability in image denoising. Section II-B presents the proposed parameters models and its calculation methods, to weight the diffusion equation. Section II-C presents the proposed diffusion speckle reduction and denoising method, the scatterer density weighted nonlinear diffusion method (SDWND). Section II-C includes the way the diffusion equation is solved, explaining the proposed diffusivity function, diffusion parameters used in different experiments, automatic stopping criteria, proposed algorithm, and the equations of the existing image quality and edge quality measures. The experimental analysis, results, and evaluation are presented in Section III. Finally, Section IV gives conclusions and suggestions for future work.

II. NON LINEAR DIFFUSION

A. Nonlinear Diffusion in Image Denoising

Diffusion is intuitively regarded as a physical process that equilibrates concentration differences without creating or destroying mass. This physical observation can be easily cast in a mathematical formulation. If u is the concentration and C is the diffusivity function, then the diffusion equation is given as:

$$\partial_t u = div(C\nabla u) \qquad (1)$$

In image processing we may identify the concentration u with the grey value at a certain location. If the diffusivity function C is constant over the whole image domain, one speaks of *homogeneous* diffusion, and a space-dependent filtering is called *inhomogeneous*. Often the diffusivity function is a function of the differential structure of the evolving image itself. Such a feedback leads to *nonlinear diffusion* filters.

The diffusion-based filter calculates a filtered image *u(x,y,t)* of the original noisy image *f(x,y)* as a solution to the nonlinear diffusion equation as shown:

$$\partial_t u = div(C(x, y)\nabla u), \qquad (2)$$

with the original image *f(x,y)* as the initial state:

$$u(x,y,0)=f(x,y), \qquad (3)$$

and reflecting boundary conditions on the image boundary:

$$\partial_n u := 0, \qquad (4)$$

where n denotes the normal to the image boundary. The nonlinear diffusivity function *C(x,y)* is usually given as a strictly decreasing function of the magnitude of the gradient.

B. Ultrasound Image Features Weighted Nonlinear Diffusion

Perona and Malik [9] suggested incorporating the image gradient into image diffusion-based filtering scheme to produce adaptive edge-preserving image filters. Since then, many researchers [10-16] have suggested improvements and modifications related to the form of the diffusivity function and the terms of the diffusion PDE [17-18,27-28]. However, diffusion schemes that depend on other factors of physical importance haven't received much attention in literature.

Here, we investigate the effect of important image features on the performance of ultrasound image diffusion scheme. The features, namely the image gradient (G), and the proposed ultrasound scatterer density parameter (α) at different regions in the image, describe edges and scatterer density properties along different geometric structures in the image.

1. Image Gradient

Gradient edge detection is the most widely used technique to weight the nonlinear diffusion filters. Here, the image f (x,y) , $(x,y) \in R^2$, is convolved with only two kernels, one estimating the gradient in the x-direction, Gx, the other is the gradient in the y-direction, Gy. The absolute gradient magnitude is given by:

$$|\nabla f| = \sqrt{G_x^2 + G_y^2} , \qquad (5)$$

2. Ultrasound Speckle Patterns and Scatterer Density

The Rayleigh distribution models the scatterer density where a large (infinite) number of uniformly distributed small size scatterers (compared to the wavelength of the ultrasound wave) are present. But this scenario is satisfied in very limited situations [14]. In general, the "effective" number of scatterers is finite. Thus there is a need to model the situation with smaller scatterer density. A general distribution that accounts for small scatterer density was proposed by V. Dutt in [5,19]. The envelope of the received backscattered signal A can be evaluated as:

$$p(A) = 2\left(\frac{A}{2}\right)^{\alpha} \frac{b^{\alpha+1}}{\Gamma(\alpha)} K_{\alpha-1}(bA), \qquad (6)$$

where $b = \sqrt{\dfrac{4\alpha}{E\{A^2\}}}$ and $K_{\beta}()$ is the modified Bessel function of the second kind of order β.

This distribution is the so-called the K distribution. It gives a generalization of the Rayleigh distribution to account for small scatterer density. Dutt shows that the parameter α of the envelope of the amplitude density function could be treated as the "effective" number of scatterers per resolution cell. Next, we show how to evaluate this parameter from the K distribution moments [5-19].
The moments of K distributed data have a closed form expression as:

$$E\{A^{\eta}\} = \frac{(2\sigma^2)^{\eta/2}\Gamma(1+\eta/2)\Gamma(\alpha+\eta/2)}{\alpha^{\eta/2}\Gamma(\alpha)} \qquad (7)$$

Because the moments have closed form expressions, one can devise methods of estimating the parameters of K distributed data based on sample moments estimated from the data. Several methods have been proposed to estimate α from normalized moments [6]. A method that employs lower order moments is the method of the second- and fourth-order moments. This method is as follows. Using (7), the normalized ratio of the fourth moment to the second moment squared can be written as:

$$\frac{E\{A^4\}}{E^2\{A^2\}} = 2(1+\frac{1}{\alpha}) \qquad (8)$$

This equation suggests an estimate for α using the sample fourth-order moment, μ_4, and second-order moment, μ_2 , as:

$$\hat{\alpha} = \frac{2}{\dfrac{\mu_4}{\mu_2} - 2} , \qquad (9)$$

where the sample moments are given by:

$$\mu_{\nu} = \frac{1}{N}\sum_{i=1}^{N} A_i^{\nu} , \qquad (10)$$

where the A_i are the N samples of the envelope of the received backscattered signal used to estimate the parameters of the K distributed data from fourth-order moment, μ_4, and second-order moment, μ_2 for a window of size WxW. μ_2 and μ_4 can be directly calculated from the window histogram. The scatterer density parameter (α) was used in the characterization of reperfused infracted myocardium from high frequency intracardiac ultrasound imaging [36-38] for large window size of 33x32 for a range of α from 2 to 15 for the myocardium region. This research [36-38] showed significant results that characterize the normal from infracted myocardium. In our method a smaller windows of size 3x3, 5x5, 7x7, 9x9, and 11x11 are studied. We also calculate the average α value (α_{ov}) for the whole image as a global measure of the evolution of the diffusion equation weighted by α. In SDWND method, we propose to weight the diffusion process with the gradient and scatterer density, thus covering whole information contents of structure geometry and scatterer density that models the speckle patterns of the K-distribution.

C. Flow of the Diffusion Denoising Process

The diffusion equation can be written in the general form as:

$$\frac{\partial}{\partial t}U(x,y,t) = \nabla \bullet (C(x,y,t)\nabla U(x,y,t)) \qquad (11)$$

where "$\bullet$" represents the inner product of two vectors. When C is a constant, the diffusion process is isotropic. When C is a function of the directional parameters, the process becomes anisotropic. To solve the above partial differential equation (PDE), the original image u_o is used as the initial condition and the Neumann boundary condition is applied to the image borders:

$$u(x,y,t)_{t=0}=u_o=f(x,y) , \quad \partial_n u=0. \qquad (12)$$

The Neumann boundary condition avoids the energy loss in the image boundary during the evolution of the diffusion process. There are some common diffusivity functions [18] in the literature. Some of these functions are shown below:

Perona-Malik 1: $\quad C(x,y,t) = 1/(1+\dfrac{|\nabla U_{\sigma}|^2}{K^2}) \qquad (13)$

Perona-Malik 2: $\quad C(x,y,t) = \exp(-|\nabla U_{\sigma}|^2 / 2K^2) \qquad (14)$

Charbonnier: $\quad C(x,y,t) = \left(1+\dfrac{|\nabla U_{\sigma}|^2}{K^2}\right)^{-1/2} \qquad (15)$

Weikert (with m=2, 3, and 4)

$$C(x,y,t) = \begin{cases} 1 & If\,|\nabla U_{\sigma}| = 0 \\ 1-\exp(-\dfrac{Cm}{(|\nabla U_{\sigma}|^2 / K^2)^m}) & If\,|\nabla U_{\sigma}| > 0 \end{cases} \qquad (16)$$

where $\quad 1 = \exp(-C_m)(1+2C_m m) \qquad (17)$

For $m=2$, 3, and 4, $C_m=2.33666$, 2.9183, and 3.31488.

$C(x,y,t)$ varies as anisotropic scalar function of the image data, and is small where the gradient of the image is large, resulting in lower diffusivity near the edges. The conductance parameter K enables backward diffusion [17] when it is smaller than the gradient ∇U_σ, thus enhancing the edges. As the image is smoothed, and the unwanted intensity variations diminish faster than the signal, the gradient measurements become more reliable. The early work of Perona-Malik resulted in an ill-posed problem, where images close to each other could produce divergent solutions and very different edges [17]. The common solution to this problem was to use a regularized (smoothed) version of the image to calculate the gradient in (13-16). Thus we calculated the gradient using the regularized version by the following equation:

$$\nabla U_\sigma = \nabla(G_{\sigma_\tau} * U(x,y,t)), \tag{18}$$

where $G_{\sigma\tau} *$ is the Gaussian convolution with the image. The gradient is taken after the image at time t is smoothed by convolution with a Gaussian of standard deviation σ_τ. The parameter σ_τ can be decreased with time evolution however in our experiments we kept it constant and equal to one (the order of one pixel size) through the evolution of the diffusion process.

1. Solution of the Diffusion Equation

We followed Weickert's method [12,27] to solve the nonlinear diffusion equation.

The *1D* diffusion equation is given as:

$$\partial_t u = \partial_x(C(|\partial_x u_\sigma|^2)\partial_x u) \tag{19}$$

The explicit scheme resulted from the discretization of nonlinear equation yields:

$$u^{k+1} = u^k + \tau A(u^k)u^k, \tag{20}$$

where u^{k+1}, and u^k are the u values at iterations k and $k+1$ of time step size τ, where discrete time $t_k=k.\tau$. The distance between the centers of the *pixels(i,j)*, referred to as the grid spacing, is h.

The elements of the matrix $A(u^k)$ are defined as:

$$A(u^k) = [a_{ij}(u^k)] = \begin{cases} \frac{C(j,k)+C(i,k)}{2h^2} & for \quad j=i-1 \, and \, j=i+1 \\ \frac{C(i-1,k)+C(i,k)}{2h^2} - \frac{C(i+1,k)+C(i,k)}{2h^2} & for \quad j=i \\ 0 & otherwise \end{cases} \tag{21}$$

The semi-implicit scheme resulted from the discretization of nonlinear equation yields:

$$\frac{u^{k+1} - u^k}{\tau} = A(u^k)u^{k+1} \tag{22}$$

This leads to the scheme:

$$\{I - \tau A(u^k)\}u^{k+1} = u^k \tag{23}$$

The *2D* equation discretization gives rise to the explicit equation:

$$u^{k+1} = u^k + \tau\{A_x(u^k) + A_y(u^k)\}u^k \tag{24}$$

and gives rise to the semi-implicit discretization:

$$\{I - \tau(A_x(u^k) + A_y(u^k))\}u^{k+1} = u^k \tag{25}$$

A is a tridiagonal matrix, with nonzeros along the main diagonal ($j=i$), the first super-diagonal ($j=i+1$) and the first sub-diagonal ($j=i-1$), where i is the row number and j is the column number in the matrix. As a result of this sparsity, the matrix-vector multiply requires few operations and the explicit approach is computationally very efficient. However, it requires small time steps for stability. As a result, more time steps are required to reach a particular time t_k. The semi-implicit scheme doesn't give the solution $u[k+1]$ explicitly. It requires solving a linear system first. So, it is called a linear-implicit (semi-implicit) scheme. The main advantage of this scheme is that it is stable for large time steps,

$$\tau = T_k/k_n \tag{26}$$

Where τ is the time step size and T_k is the discrete time where $k_n \in IN_0$ is the number of iterations. Higher τ means more diffusion however Weickert [27,18] and others stated that many nonlinear diffusion problems require only the elimination of noise and some small-scale details. Often this can be accomplished with τ not more than 5. Solving the system of equations was performed using Thomas algorithm, which is a Gaussian elimination algorithm for tridiagonal systems. The update equation used in 2D case is the semi-implicit scheme, using additive operator splitting (*AOS*) given as:

$$u^{k+1} = \frac{1}{2}\{(I - 2\tau(A_x(u^k))^{-1} + (I - 2\tau(A_y(u^k))^{-1})\}u^k \tag{27}$$

This reduces to the solution of two tridiagonal systems. This operator is first order accurate in time and the *AOS* scheme is stable for large time steps. The semi-implicit scheme has shown unconditional stability in the scalar nonlinear anisotropic diffusion for any time step.

2. Proposed Diffusivity Function

We propose the diffusivity function $C(x,y,t)$ given as:

$$C(x,y,t) = C(\alpha \bullet |\nabla U|), \tag{28}$$

where "•" is the product operator. Using any of the diffusivity functions in the literature, for example Perona-Malik 1, and extending this function to include a weighted α, for local region, in addition to the gradient, thus $C(x,y,t)$ becomes:

$$C(x,y,t) = 1/(1 + \frac{(\alpha.|\nabla U_\sigma|)^2}{K^2}) \tag{29}$$

This equation weights the diffusivity function with gradient magnitude and the proposed scatterer density measure (α), which are locally calculated for a window WxW. The function $C(x,y,t)$ is estimated at each time, *t,* of the diffusion process and can take any form of the monotonically decreasing diffusivity functions in the literature. Our diffusivity function is anisotropic in the sense that it varies at each point in the image surrounded by local region WxW and with the degree of anisotropy in the gradient (edge extent) and scatterer density (speckle patterns). It is implemented in *2D* as in (21 and 27) as a function of directions, yet it is not in a tensor formulation as in [14,18]. According to Weickert, it can be modified to a tensor formulation as in [18] assuming $\lambda_2=1$ and λ_1=our $C(x,y,t)$ defined in (29). In this paper we studied only the isotropic case and the tensor formulation for both edge preservation and coherence enhancement is currently under

study. The proposed model does not only preserve edges but also reduce speckle noise by incorporating the local tissue α into the diffusivity equation. From the functional point of view, diffusivity function combines both isotropic and anisotropic diffusions. According to the extent of the local speckle regions and image anisotropy, the function changes from isotropic diffusion to anisotropic one. In homogenous regions where there is low information described by the gradient magnitude as a measure of the edges, and α as a measure of scatterer density forming speckle pattern, the diffusion process reduces to isotropic one. In the case of regions of high information contained in the parameters with different weights, especially at edges, interfaces, vessels, speckled and textured regions, the diffusion process is anisotropic as a function of these parameters, thus operating adaptively depending on the relative contents of these parameters in the locally analyzed regions.

3. Image Quality Measures

The RMSE, SNR, and PSNR are image quality measures and are given as:

$$RMSE = (\frac{1}{NM}\sum_{i=1}^{N}\sum_{j=1}^{M}(u_{original}(i,j) - u_{denoised}(i,j))^2)^{1/2} \qquad (30)$$

$$PSNR(dB) = 20\log_{10}(1/RMSE) \qquad (31)$$

$$SNR(dB) = 10\log_{10}(\sigma_u^2 / \sigma_e^2) \qquad (32)$$

$$\sigma_e^2 = (\frac{1}{NM}\sum_{i=1}^{N}\sum_{j=1}^{M}|u_{original}(i,j) - u_{denoised}(i,j)|^2) \qquad (33)$$

where σ_u^2 is the variance of the denoised image.

In addition to these image quality measures, we calculated the universal image quality index (Q) defined in [41], where it measures the distortion between two images (noise free and noisy images), modeled as a combination of three factors, the loss of correlation, luminance distortion, and contrast distortion. In our analysis, we computed Q as an average of all Q values at each pixel. The local Q value for each pixel is calculated for a sliding window of 8x8 as in [40-41]. The dynamic range of Q is between [-1,1], the best value of Q=1 is achieved if and only if the two images are equal. The higher the Q values, the less the distortion between the original and the processed image is. In our experiments, we calculated SNR, PSNR, and Q for a grey-scale images normalized from 0-255 grey-scales to 0-1. In addition to these measures, we calculated the α_{ov}, to be added to these image quality measures to evaluate the degree of diffusion process. The quantitative measure of edge preserving or edge enhancement is calculated by the Pratt's figure of merit (FOM), to give a quantitative evaluation, and is defined in [42]. In calculating FOM, we used the λ parameter to be 1/9. The dynamic range of FOM is between [0,1]. Higher FOM value indicates better edge matching between processed and ideal image. In calculating FOM, we used the resulted Canny edge map of the diffused image and compared it to the ideal phantom reference Canny edge map image. Now we have quantitative and qualitative evaluations for both image quality and edge preservation. The SNR, PSNR, and Q are the quantitative evaluation of image quality. The diffused images with evolution of diffusion process and the 2D maps of different parameters are

qualitative measures of image quality. The quantitative measure of edge preservation is the FOM measure. The qualitative measures of edges are the Canny edge map and the gradient map. In order to have an overall index for image and segmentation quality, let us define the following index as:

$$\gamma = Q \bullet FOM \qquad (34)$$

This index, γ, is an overall image and segmentation quality index.

4. Diffusion Parameters

We followed Weickert's rule-of-thumb in his paper [27] where he stated that many nonlinear diffusion problems require only the elimination of noise and some small-scale details. Often this can be accomplished with no more than 5 discrete time steps. So in some experiments we fixed τ to be equal to 5 in order to see the effect of weighting the diffusivity function with the new proposed image parameters. The conductance parameter, K, can be used as a time varying function as in [28] in order to cool down the system. The value of K is used to balance the amount of forward diffusion (where everything is smoothed) and backward diffusion (where contrast enhancement is happened). We have tested the algorithm for different values of τ. We measured the quality of diffusion in SNR, PSNR, Q, FOM, γ, α, the detected canny edge map, and the visual inspection of the diffused image, and the 2D maps for α and gradient, and the evolution of the overall image average scatterer density(α_{ov}). The denoising process is accomplished with good compromise between efficiency and accuracy for $\tau=3-5$, similar to what Weickert observed [12,27]. We have tested the effect of time step size τ on the diffusion process and we have found our experiment agree with Weickert who stated that we can achieve a good denoising (a compromise between efficiency and accuracy) in no more than 5 discrete time steps. We have adopted the *AOS* algorithm illustrated in [12] in the *2D* case in (27) and by replacing the diffusivity matrix with our proposed equation (29). We fixed the value for the grid size h_1 and h_2 equal to 1, since all the test and clinical images have an aspect ratio of 1. We have studied the dependence on the conductance, K, and got the compromized value that allows forward and backward diffusion processes, and then we used it in other experiments.

5. Proposed Stopping Function

In our experimental result of varying τ, and using the diffusivity function shown in (29), we found that it can be achieved for $\tau \leq 5$. The noise is completely removed as in Figs. 2-3 and this is shown in the time evolution curve of Fig. 4, which shows the α_{ov} with iterations, as well, with the progress of other quality measures (SNR, PSNR, Q, FOM, and γ). According to Weickert's criteria, our findings, and observation of the scatterer density and overall image and segmentation quality (γ) behaviors with different values of τ and iterations, we propose the following time varying stopping function to stop the diffusion process as a function of consecutive quality measures. Since when no major γ or α_{ov} variations occur between two consecutive discrete time steps (equilibrium state) is equivalent to some quality measure

between two consecutive diffused images, we propose the following normalized criteria to stop the ultrasound denoising process:

$$\left| \frac{\gamma(k+1).\alpha_{ov}(k+1) - \gamma(k).\alpha_{ov}(k)}{\gamma(0).\alpha_{ov}(0)} \right| < \delta \qquad (35)$$

where $\gamma(k+1)$ and $\gamma(k)$ are the overall image and segmentation quality at iterations $k+1$ and k, respectively. $\gamma(0)$ is the initial overall image and segmentation quality of the noisy speckled image. $\alpha_{ov}(k+1)$ and $\alpha_{ov}(k)$ are the overall average image scatterer densities at iterations $k+1$ and k, respectively. $\alpha_{ov}(0)$ is the initial image average scatterer density of the noisy speckled image. The parameter, δ, is defined as a certain threshold to stop the diffusion process. The value of δ was experimentally found to be in the range of 2-3% for different ultrasound test phantom and clinical images of different speckle patterns. So the diffusion process will stop whenever this condition ($\delta < 3\%$) or stopping time is reached. This δ value $< 3\%$, between two consecutive diffused images is equivalent to a change in PSNR(dB) <0.5 dB.

6. Proposed Algorithm

An iteration k, of the proposed algorithm consists of the following steps:

Step 1) Convolve the image with G_σ of one standard deviation as in (18), for $\sigma=1$, $h_1=h_2=1$, $\tau=5$. For a compromised value for conductance (K), let $\delta=3\%$.

Step 2) For each point (x,y) that belong to 2-D space of all real numbers, $(x,y) \in \Re^2$, calculate the gradient magnitude as in (5) and overall image and segmentation quality, γ, as in (34) for local window of size WxW.

Step 3) Calculate the Diffusivity matrix, C(x,y,t) at iteration k, as in (29).

Step 4) Construct the A_x and A_y matrices as in (21) from the calculated C(x,y,t) at iteration k.

Step 5) Solve the diffusion equation in (27), to update u($k+1$) from u(k) and the calculated matrices at step k, using the semi-implicit scheme with additive operator splitting (AOS).

Step 6) Finish the whole points in the image then calculate $\gamma(k)$ and $\alpha_{ov}(k)$, and check for the stopping criteria (δ) as in (35) as a function of k.

Step 7) Loop until either stopping criteria in (35) is satisfied or discrete time, T_k, as in (26) is reached.

It is obvious from the shown algorithm that the diffusivity function is updated with the resulted gradient and scatterer density for each local region of the diffused image, for each individual step k. Also $\delta(k)$ is calculated at each iteration. A minimum number of iterations is 1 in order to calculate $\delta(0)$ from $\gamma(1)$ of the diffused image at iteration 1 and $\gamma(0)$ of the original image.

III. EXPERIMENTAL RESULTS AND EVALUATION

We investigated and tested the performance of the proposed nonlinear diffusion method (SWDNAD) on reducing the speckle noise for test phantom and clinical ultrasound images using all possible combinations of two factors: the image

gradient and the scatterer density. We have conducted the following experiments in order to select the best choice of diffusivity weighting function of our proposed method. That is, we tested the performance using each factor alone and two at a time. To compare the performance for different choices of diffusivities, we used these set of image quality measures (SNR, PSNR, and Q), edge preservation (FOM), overall image and segmentation quality index (γ), and Canny edge detector map in addition to the evolution of α_{ov}, scatterer density maps, and gradient maps with time steps. The default (if not specified in some experiments) diffusion parameters were set as, $\sigma=1$, $K=0.5$, $h_1=h_2=1$, $\tau=5$, $T=25$, Perona-Malik 1 function, 3x3 window, *AOS* scheme, and with 5 iterations.

A. Test Images

In our experiments, we used a contrast detail phantom image (ATS laboratories, Bridgeport, CT). The contrast detail phantom was made to produce standard contrast levels from −15 dB to +12 dB. The phantom image has a resolution of 256×128 and consists of eight different contrast regions (four positive contrast regions and four negative contrast regions). Regions are ordered in two rows. The upper row contains negative contrast regions while the lower one contains the positive contrast regions as shown in Fig. 1. A reference image was constructed manually from the speckled image by evaluating the mean value in each region [14]. All images were acquired at 3.5 Mhz.

B. 2D Maps for Contrast Detail Image

Fig. 2 shows the evolution of the diffused phantom image for 5 iterations of $\tau=5$. Fig. 3 shows the associated Canny edge maps of the diffused images. Fig. 3 shows the amount of enhancement of the edge map started with the evolution of the process for each iteration. Canny edge maps of Fig. 3 show that the contrast circles simulating ultrasound hyper positive contrast and hypo echoic negative contrast structures in the phantom image, started to appear clearly at iterations 4-5. The process started with a non-meaningful edge map of the original image and ended with a meaningful Canny edge map after 4-5 iterations. At iteration 5, it is shown from Fig. 5 that the major scatterer regions are around the 8 contrast circles due to the large number of scattering found at the interfaces between different tissue. In ultrasound imaging, different distribution of collagen, elastic fibers, and vessels containing blood is one of the major sources of scattering of the ultrasound beam. Fig. 4 shows the scatterer density evolution with the 5 iterations. There is a progressive decrease in the value of the image α_{ov} from 0.6518, 0.4026, 0.3146, 2691, 0.2438, to 0.2249 after 5 iterations, which represents a 34.5 % of the original α_{ov} value. The Q values decreases from 1, 0.8476, 0.6312, 0.4692, 0.3598, to 0.2860. The FOM changes from 0.1813, 0.176, 0.1763, 0.1886, 0.2045, to 0.2163. The γ value changes from 0.1813, 0.14473, 0.1112, 0.08849, 0.0735, to 0.0618. The δ calculated values for the 5 iterations are 21.35%, 8.36%, 4.02%, 2.11%, and 1.44%. In our stopping criteria defined in (35), we proposed to stop the diffusion process at iteration 4 since it satisfies the quantitative value of the defined stopping threshold ($\delta<3\%$).

This value was empirically suitable for most clinical ultrasound images experimented.

C. Conductance Parameter (K) Choice on SDWND

The conductance parameter *K* represents the steepness of the decreasing monotonically diffusivity function. The value of K is used to balance the amount of forward diffusion (where everything is smoothed, $K \geq |G.\alpha|$) and backward diffusion (where edge contrast enhancement is happened, $K < |U_\sigma.\alpha|$). To study the performance of the diffusion process with different conductance values of K=0.001,0.01,0.1 0.2, 0.3, 0.4, 0.5, 0.6, 0.7, 0.8, 0.9, 1, 1.5, 2, 10, 100, and 1000. We conducted the following experiment for $\tau = 5$ and for 5 iterations, for Perona-Malik 1 function with *AOS* scheme, and using other default values in section III. Table I shows the effect of the conductance parameter on the quality diffusion of the process. For K=10, 100, and 1000, the results are unchanged since (forward diffusion where everything is smoothed, $K > |U_\sigma.\alpha|$). Figs. 6-7 show the resulted diffusion images and its associated Canny edge maps. We can observe that the K interval in which there is a smoothing and edge preservation is between 0.1 and 2. Fig. 8 show plots of Q, FOM, γ, and α_{ov} versus K for the three diffusivity functions in (36-38). Fig. 8-a shows Q as a decreasing function with K. Fig. 8-b shows FOM as an increasing function with K. Fig. 8-c shows γ as a decreasing function with K. Fig. 8-d shows α_{ov} as a decreasing function with K. The value for K that show a compromise for smoothing and edge preservation was selected at K=0.5.

TABLE I
SNR, PSNR, Q, FOM, Γ, AND A_{ov} COMPARISON WITH DIFFERENT CONDUCTANCE K, FOR ORIGINAL CONTRAST DETAIL PHANTOM IMAGE OF ORIGINAL A_{ov} = 0.6518, FOM WITH IDEAL=0.18131, Q WITH IDEAL =0.04635

K	SNR	PSNR	Q	FOM	γ	α_{ov}
0.001	24.927	45.194	0.994	0.181	0.180	0.6309
0.01	16.349	36.616	0.963	0.182	0.176	0.5458
0.1	8.167	28.434	0.707	0.188	0.133	0.361
0.2	6.039	26.306	0.506	0.196	0.099	0.2944
0.3	5.13	25.397	0.391	0.202	0.079	0.2600
0.4	4.663	24.929	0.326	0.211	0.069	0.239
0.5	4.379	24.646	0.286	0.216	0.062	0.2249
0.6	4.191	24.458	0.26	0.221	0.057	0.2155
0.7	4.062	24.329	0.242	0.220	0.053	0.2089
0.8	3.97	24.237	0.231	0.211	0.051	0.2044
0.9	3.898	24.165	0.221	0.242	0.053	0.2021
1	3.84	24.107	0.214	0.239	0.051	0.2002
1.5	3.691	23.958	0.197	0.250	0.049	0.196
2	3.63	23.897	0.19	0.252	0.048	0.1942
10	3.545	23.812	0.181	0.272	0.049	0.1925
100	3.541	23.808	0.181	0.271	0.049	0.1924
1000	3.541	23.808	0.181	0.271	0.049	0.1924

D. Comparison between Linear and Nonlinear Diffusions

In this experiment, we compared the performance of linear isotropic ($D\equiv1$ as Gaussian filter) and nonlinear diffusions weighted by (29). The diffusion parameters were set as σ=1, K=0.5, h1=h2=1, τ=5, T=25, Perona-Malik 1 function with AOS scheme. This was set for gradient and all parameters diffusion while in Gaussian removal using the Gaussian convolution with standard deviation σ, is equivalent to linear diffusion filtering (D=1) for some time T= σ²/2 for one time

step as in [12], for linear diffusion and with using *AOS* stable scheme, and taking into our considerations of σ to be in the order of the pixel size.

Table II and Figs. 9-10 show an overall enhancement of the different quality measures by the three methods compared with the quality measure between the phantom image and the reference image. However a slight decrease of image quality measures of the phantom occurred, we achieved the highest FOM value when the diffusion equation was weighted by our method of diffusivity (all parameters), as there is an increase of the FOM value of 0.2163 when weighted by (29) compared to 0.1776 for Gaussian linear filter, and 0.201 when weighted by Gradient nonlinear diffusion only. Fig. 7 shows how the phantom image has a vague edge map and how the best edge map was achieved when we weight the diffusivity function by the two parameters. Since the highest FOM for the phantom image was obtained when incorporating the two parameters into the diffusivity function and the difference in the different quality measures is very small (< 0.5 dB PSNR) as observed in the visual quality of images, we studied different choices of parameters in diffusivity function on the performance of the diffusion process in section III-F. However both Gaussian processes in the phantom images have a higher quality measures, it is not suitable for any automatic segmentation or active contour processes (lower FOM value, vaguer edge map, and Gaussian filter changes the position of edges) while the images diffused using (29) have higher FOM, better edge map, and is suitable for automatic segmentation issues.

TABLE II
COMPARISON BETWEEN QUALITY MEASURES AND THE PROPOSED SCATTERER DENSITY MEASURE FOR ULTRASOUND DIFFUSION PROCESS OF PHANTOM IMAGE OF ORIGINAL A_{ov} = 0.6518, FOM WITH IDEAL =0.18131, Q WITH IDEAL =0.04635

Diffusion	SNR	PSNR	Q	FOM	γ	α_{ov}
Gaussian	6.547	26.914	0.615	0.177	0.109	0.3393
$\left\lvert \nabla U_\sigma \right\rvert$	4.821	25.088	0.352	0.201	0.070	0.2487
$\left\lvert \nabla U_\sigma \right\rvert .\alpha$	4.379	24.646	0.286	0.216	0.062	0.2249

E. SDWND in Removing Noise and Preserving Edges

In order to evaluate the capability of the SDWND in removing noise with preserving edges and image features, we have chosen some clinical test ultrasound images for fetal face (Fig. 11 of 580x433 pixels), heart (Fig. 12 of 256x256 pixels), and phantom reference (Fig. 13 of 256x128 pixels) of different edges, texture, speckle, and scattering properties. In order to evaluate the effects of applying our diffusion-based denoising filter, we have added Gaussian noise, with standard deviation of 20, to each of the images shown in Figs 11-13. Using diffusion parameters set as σ=1, K=0.5, h1=h2=1, τ=5, T=25, Perona-Malik 1 function, and with AOS scheme. The diffusion process using our proposed method is applied to the noisy images. The effectiveness in removing the noise is obtained by different quality measures, edge measures, and the 2D edge, gradient and scatterer density maps. The performance results in Table III show the capability of the proposed SDWND method to reduce the noise in all the clinical and test noisy images, and do so without blurring or

changing the location of the edges as well to preserve basic image features as shown in the resulted denoised images with its associated Canny edge maps. The original Canny edge maps for the whole images are quite vague and not suitable at all for automatic segmentation process, while the resulted Canny edge maps of the SDWND diffused images show significant edge enhancement and edge preservation of the different original anatomy.

TABLE III
SNR, PSNR, AND Q COMPARISON O FIGS.(11-16), USING DIFFUSIVITY IN (29)

Images	SNR	PSNR	Q
Face before denoising	2.784	19.406	0.1568
Face after denoising	5.888	23.005	0.2232
Heart before denoising	4.926	18.726	0.2351
Heart after denoising	7.947	21.747	0.3201
Phantom Reference before densoising	-2.818	20.635	0.0647
Phantom Reference after densoising	10.794	34.248	0.1952

Figs. 11-13 show these difficulties on the noisy images to track shapes of the anatomy of fetal face in Fig. 11 for automatic 3D segmentation and 3D rendering of fetal face, heart chambers with valves in Fig. 12 for volumetric 4D measurements and analysis of the valves patterns in 4D, and hypoechoic structures of negative contrast simulating vessels and hyperechoic structures of positive contrast simulating tumors in Fig. 13, which is used in B-mode ultrasound machines calibration and quality control, to determine and calibrate ultrasound machine parameters and thus correcting measurements (area/volume). In Figs. 14-16, it is easy to segment and detect these anatomical shapes as it is clearly shown in its associated canny edge maps. In Figs. 13 and 16, it is observed that the circular contrast structures in the phantom reference image are clearly delineated and edge detected which was not clear in the edge map of Fig. 13. The resulted gradient and scatterer density maps show the relative contents of these features in the noisy reference image, where the resulted image has a small number of scatterer density per unit cell and the image contains clear gradient structures of those circles. Table III shows a remarkable increase of the SNR, PSNR, and Q for before and after denoising of the phantom reference and other clinical images. Figs. 14-16, the basic gradient of the important structures of the anatomy is preserved with the important texture information contained in the varieties of the shown texture images. Thus, the active contour process will remain stuck in ambiguous contours of Figs 11-13 due to the existence of the noise. Also in cases of automatic detection of 2D or 3D objects of *a priori* known shapes with any method such as Hough transform, it will be easier to detect predefined anatomical shapes (vessels, heart chambers shape, fetal head, fetal face, and contrast circles), when we apply the diffusion process to the noisy images. It is more accurate to calculate automatic 3D volumetric measurements to predict, for example, expected fetal birth date, to quantify some heart diseases with the 4D calculation of 3D volumes with cardiac cycles, and to quantify some 3D volumetrics for a hypo or hyperechoic tumors for further surgical planning or treatment.

F. Choice of Parameters in Weighting SDWND

To select the best choice of diffusivity function, we applied the following experiments on the contrast detail phantom image, using Perona-Malik-1 with the default diffusion parameters set as in section III of $\sigma=1$, $K=0.5$, $h_1=h_2=1$, $\tau=5$, $T=25$, 3x3 window, *AOS* scheme, and with 5 iterations. We tested the following three normalized functions for standard gradient weighting, scatterer density weighting, and the multiplication of both on the diffusion quality (Image and segmentation quality).

$$C(x,y,t) = 1/(1+\frac{|\nabla U_\sigma|^2}{K^2}) \qquad (36)$$

$$C(x,y,t) = 1/(1+\frac{\alpha^2}{K^2}) \qquad (37)$$

$$C(x,y,t) = 1/(1+\frac{(\alpha.|\nabla U_\sigma|)^2}{K^2}) \qquad (38)$$

Table IV, Fig. 17, and Fig. 8 at k=0.5 show the results of using these three functions to weight the diffusion of the phantom image. We observed that the phantom image has experienced a progressive increase in the image quality and segmentation quality and experienced a decrease in the α_{ov} as time evolves. The result shows that the diffusion using the scatterer density only can essentially perform equally or better than the diffusion depending on the gradient only. The image quality measures using scatterer density alone has the highest values. However, the gradient is an indispensable factor that should be present in the diffusivity weighting. The highest FOM value was achieved for the function shown in (38) which shows the importance of adding the scatterer density in the diffusivity function. We concluded that by incorporating the gradient magnitude multiplied by the scatterer density into the diffusivity function, we can gain better performance in terms of noise removal and edge preservation. Table IV shows that the phantom noisy image has experienced a progressive decrease in the α_{ov} as time evolves. Also the α_{ov} of the diffused phantom image has experienced a very small decrease compared to gradient weighting alone.

TABLE IV
SNR, PSNR, Q, FOM, Γ, AND A$_{ov}$ COMPARISON OF DIFFERENT CHOICES OF DIFFUSIVITY PARAMETERS FOR ORIGINAL CONTRAST DETAIL PHANTOM IMAGE OF ORIGINAL A$_{ov}$ = 0.6518, FOM WITH IDEAL =0.18131, Q WITH IDEAL =0.04635

Parameters	SNR	PSNR	Q	FOM	γ	α$_{ov}$
$|\nabla U_\sigma|$	4.821	25.088	0.352	0.201	0.071	0.2487
α	4.806	25.073	0.36	0.205	0.074	0.2449
$|\nabla U_\sigma|.\alpha$	4.379	24.646	0.286	0.216	0.062	0.2249

G. Performance of Proposed Choices of Diffusivity Function

Table IV shows the performance measures (SNR, PSNR, Q, FOM, γ), in addition to the α_{ov} for different choices of diffusivities weighted by different parameters, for the phantom image. However, the higher measures do not always mean better quality [24,40]. Table IV showed that the highest FOM (edge preserving and edge enhancement measure) is for the gradient and scatterer density weighted while the highest

quality measures (image distortion measures) are for the scatterer density weighted and the gradient weighted. This result assures the importance of scatterer density in weighting the diffusivity function. In edge preservation, we achieved the highest value when we incorporated the scatterer density with the gradient. The actual value of the quality measures is not physically meaningful, but the comparison between two values for different diffused or reconstructed images gives one measure of reconstructed or processed quality. Using PSNR measure for example in image reconstruction, the MPEG committee used an informal threshold of 0.5 dB PSNR to decide whether to incorporate a coding optimization since they believed that any improvement of that magnitude would be visible. However, the differences in PSNR values do not exceed 0.5 dB, we have an enhanced denoised visible image of good edge map sharpness that can be suitable as a preprocessing step for further segmentation or active contour processes of organs, tumors, or vessels. In analyzing ultrasound images when only texture information can present as in the hepatic parenchyma of non-randomly distributed speckle patterns with long-range order (NRLR) [5,43,44], it is not wise to weight the diffusivity function with the gradient alone since the gradient will be a noisy information. When we have the whole information contained as a texture due to speckle noise, in organ surfaces and blood vessels images that contain non-randomly distributed speckle patterns with short-range order (NRSR) [43], scatterer density weighting can perform better than the gradient alone. In other modalities of medical images such as MRI, CT, or PET, a different ratio of this information can occur, for example Weickert in his paper [12] analyzed MRI images which has a prominent gradient information between different tissues of brain (CSF, gray matter, white matter, and background), so weighting the diffusivity function using only gradient information was successful [12] to reduce the speckles while in ultrasound or radar images, this gradient only weighting may not be successful when not considering the speckle patterns and speckle noise formed in the texture. In other imaging modalities other than the ultrasound or radar imaging which has a speckle noise, one can propose other physical parameter, that weight the diffusion process and this can be more successful than taking the gradient alone. Lee [30] designed his filter to eliminate speckle noise while preserving edges and point features in radar imagery, Frost [31] used an exponentially damped convolution kernel that adapts to regions containing edges by exploiting local statistics, Yu and Acton [34] caste the Lee and Frost filters in the framework of the PDE bridges and unified two approaches, the PDE approach and the adaptive filtering approach, they derived their speckle reducing anisotropic diffusion method (SRAD) where [35] used this method and proposed estimation of the coefficients of variation based on the SRAD method which all were basically based only on the edges information in the PDE case. Adding the scatterer density to the diffusion weighting process showed to be successful since it is based on the K distribution model of ultrasound echoes. We have not compared our method with the several methods in the literature for speckle reduction but a few of them in section III-J, since our main goal in this paper was to propose the

scattering density into diffusivity function and show its impact on the diffusion weighting process and show the degree of anisotropy which can not be only in the gradient information that measure edginess in images, but also with scattering density which results in a different distribution of scatterers and speckle patterns within the resolution cell forming the ultrasound texture.

H. SDWND for Large Number of Iterations

To compare the performance of the SWDNAD nonlinear diffusion and linear diffusion processes for large number of iterations, we have peformed the following study using $\tau=5$, and using Perona-Malik 1 function with *AOS* scheme, for 100 iterations. For linear diffusion, it is well know that one step Gaussian convolution with standard deviation σ is equivalent to linear diffusion filtering ($D\equiv1$) for some time $T=\sigma^2/2$ as in [12] for single step linear diffusion, with using *AOS* stable scheme, and for taking into our considerations that σ is in the order of magnitude of the pixel size. In SDWND method the FOM is increasing smoothly up to 50 iterations, then decays very smoothly with small decrease at iteration 100. This FOM pattern showed the capability of the SDWND method in preserving edges without changing its position even with large number of iterations. Fig. 18 shows a decreasing pattern for α_{ov}, Q, and γ with iterations while the FOM pattern increases remarkably till iteration 25 with the largest FOM value of 0.5382 then decreases smoothly with iterations.

I. Automatic Stopping Criteria Evaluation for SDWND

To study the automatic stopping function behavior with large number of iterations, we conducted the experiment on the phantom image diffusion process, for $\tau=5$ and 100 iterations. From Figs. 18-19, our defined criteria for automatic stopping in (35), was reached after 3 iterations (value for δ=2.7% which is<3%). The associated values for the Q, FOM, γ, and α_{ov} at iteration 3 are 0.2906, 0.2065, 0.06, and 0.2143, respectively.

J. Comparison between SDWND and Other Methods

To compare the performance of our proposed SDWND method with some existing speckle reduction and coherent enhancement methods such as NCD, AWFM, WS, and WSCE, we performed the following comparison for $\tau=5$ and for 5 iterations. In our method, we used Perona-Malik 1 function with *AOS* scheme for the same settings in section III.

Figs. 20-21 and Table V show a comparison of our proposed method (SDWND) with NCD, AWFM, WS, and WCSE methods. Diffused image using SDWND have the highest SNR, PSNR, and FOM compared to all other methods. However the WS and WSCE methods has higher Q values than SDWND, it has not resolved most of the circles in the Canny edge map, the way the SDWND method did, and it has a lower FOM (edge preservation) values of 0.171 and 0.177 compared to 0.216 for the SDWND. The scatterer density value obtained with SDWND is the least value compared to all other methods. This showed the capability of the SDWND method to diffuse regions of larger scatterer density more than all other methods and remarkably preserves the edges. The resulting edge map using SDWND showed higher quality

measures and edge preservation than the NCD method. SDWND has a higher overall measure compared to NCD method. Despite the fact that NCD method is based on tensor formulation, we achieved a much better results in terms of quality measures and edge preservation. Although the diffusivity tensor provided by [14] was successful compared to AWFM, WS, and WSCE methods, it may not be effective for spatially correlated and heavy-tail distributed speckle noise [40]. In our method, we overcome this spatial correlation problem illustrated in [40] by calculating scatterer density in a window and we tested different window size in order to overcome the problem that some speckles may occupy several pixels in size. To summarize, SDWND method were capable to diffuse regions of speckle noise (reduction of speckle noise), diffuse regions of high scatterer densities, preserve edges (highest FOM), and maintain the highest quality measures compared to other methods.

TABLE V

SNR, PSNR, Q, FOM, Γ, AND A_{ov} COMPARISON BETWEEN SDWND, NCD, AWFM, WS, AND WSCE, FOR ORIGINAL CONTRAST DETAIL PHANTOM IMAGE OF ORIGINAL A_{ov} = 0.6518, FOM WITH IDEAL =0.18131, Q WITH IDEAL =0.04635

Method	SNR	PSNR	Q	FOM	γ	α_{ov}
SDWND	4.379	24.646	0.286	0.216	0.062	0.2249
NCD	3.618	23.885	0.232	0.200	0.046	0.2329
AWFM	3.712	23.979	0.264	0.184	0.049	0.2814
WS	4.127	24.393	0.381	0.171	0.065	0.2982
WSCE	3.150	23.468	0.442	0.177	0.078	0.5094

IV. DISCUSSIONS AND CONCLUSIONS

First, we proposed a new method for nonlinear anisotropic diffusion (SDWND) weighted by features extracted from ultrasound image, and have physical models related to ultrasound imaging. Second, we proposed a new algorithm with new automatic stopping criteria in order to evolve and stop the diffusion process with a good quality of the processed image measured in quantitative and qualitative image quality and edge preservation measures. Then, we tested and tuned different parameters and factors that affect the diffusion process, in order to reach the best tuning of our SDWND method for both testing phantoms and clinical ultrasound images. We investigated the performance of nonlinear diffusion filters on reducing the speckle noise with the choice of diffusivity function adding scattere density to gradient.

From our experiments, we can confirm that the introduction of scatterer density into the diffusion process increases the performance of the nonlinear diffusion process in removing the speckle noise and preserving the important structures and edges of the image. The new parameter proposed to weight the nonlinear diffusion process in addition to gradient, makes sense because they have a strong physical meaning and models related to ultrasound imaging. We also showed the better performance of our method (SDWND) as nonlinear anisotropic speckle reduction method over some of the existing methods for speckle reduction in the literature, such as NCD, AWFM, WS, and WSCE. SDWND method can be used in denoising other imaging modalities such as MRI and CT. The proposed method showed a better quality of diffusion

and better edge map compared to linear diffusion and other nonlinear tensor and non tensor based coherent enhancement diffusion methods.

SDWND can be used as a preprocessing step before applying any automatic segmentation or active contour processes. Other parameters of relative importance in modeling the speckle noise and measuring the image quality could be tested similarly for potential use, as weighting parameters of the ultrasound nonlinear diffusion filters. The codes in our experiments were implemented in Matlab version 7.04 and using a P4 machine of 2 GHz processor. The calculation of gradient, scatterer density parameters and the evolution of the diffusion process takes less than a second for the 5 iterations. Our main goal was to investigate the introduction of scatterer density in the weighting process of ultrasound diffusion denoising and evaluation of the nonlinear diffusion process. The introduction of scatterer density into the diffusion process for the isotropic case was shown to have a better performance in terms of image quality and edge preservations. We are currently studying the importance of scatterer density in edge and coherent enhancement nonlinear anisotropic diffusion methods in formulating the tensor matrix.

REFERENCES

[1] M. E. Anderson, and G. E. Trahey, "A seminar on k-space applied to medical ultrasound", *http://dukemil.egr.duke.edu/Ultrasound/k-space/* (Accessed July 1, 2006).

[2] J. C. Bamber and C. Daft, "Adaptive filtering for reduction of speckle in ultrasound pulse-echo images," *Ultrasonics*, pp. 41–44, Jan. 1986.

[3] T. Iwai, T. Asakura, "Speckle reduction in coherent information processing", *Proceedings of the IEEE*, vol. 84, no. 5, 1996.

[4] R. M. Haralick, R. Shanmugam, I. Dinstein, "Textural features for image classification," *IEEE Trans. on Systems, Man, and Cybernetics*, 3 (1973) 610–621.

[5] V. Dutt, "Statistical analysis of ultrasound echo envelope," Ph.D. dissertation, Mayo Graduate School, Rochester, MN, 1995.

[6] D. Blacknell, "Comparison of parameter estimators for K-distribution," *IEE Proceedings – Radar, Sonar Navigation*, vol. 141, pp. 45–52, Feb. 1994.

[7] J. C. Bamber and G. Cook-Martin, "Texture analysis and speckle reduction in medical echography", *SPIE*, pp. 120-127, 1987.

[8] Perona, P. and J. Malik, "Scale-space and edge detection using anisotropic diffusion", *Proceedings, IEEE Computer Society workshop on Computer Vision*, 1987, pp. 16-27.

[9] P. Perona and J. Malik, "Scale space and edge detection using anisotropic diffusion," *IEEE Trans. Pattern Anal. Machine Intell.*, vol. 12, pp. 629–639, July 1990.

[10] M. J. Black, G. Sapiro, D. H. Marimont, and D. Heeger, "Robust anisotropic diffusion," *IEEE Trans. Imag. Processing,* vol. 7, pp. 412–432, Mar. 1998.

[11] J. Weickert, "Mutiscale texture enhancement," in Lecture Notes in. Computer Science, ser. Berlin, 1995, vol. 970, *Computer Analysis of Images and Patterns*, pp. 230–237.

[12] J. Weickert et al., "Efficient and reliable schemes for nonlinear diffusion filtering," *IEEE Trans. Imag. Processing*, vol. 7, pp. 398–410, Mar. 1998.

[13] K. Z. Abd-Elmoniem, Y. M. Kadah, and A. M. Youssef, "Real time adaptive ultrasound speckle reduction and coherence enhancement," presented at the *Int. Conf. Imag. Processing* (ICIP' 2000), Vancouver, Canada.

[14] K.Z. Abd-Elmoniem, A. M. Youssef, and Y. M. Kadah, "Real-time speckle reduction and coherence enhancement in ultrasound imaging via nonlinear anisotropic diffusion", *IEEE Transaction on Biomedical Engineering*, vol. 49, no. 9, pp. 997-1014, 2002.

[15] A. Achim, A. Bezerianos, and P. Tsakalides, "Novel Baysian multiscale method for speckle removal in medical ultrasound images," *IEEE Trans. Medical Imaging*, vol. 20, pp. 772–783, Aug. 2001.

[16] R. A. Carmona and S. Zhong, "Adaptive smoothing respecting feature directions," *IEEE Trans. Image Processing*, vol. 7, pp. 353–8, Mar. 1998.

[17] Weeratunga S.K. and C. Kamath, "PDE-based non-linear diffusion techniques for denoising scientific/industrial images: An empirical study," *Proceedings, Image Processing: Algorithms and Systems, SPIE Electronic Imaging*, pp. 279-290, San Jose, January 2002.

[18] Weeratunga S.K., and C. Kamath, "A comparison of PDE-based non-linear anisotropic diffusion techniques for image denoising," *Proceedings, Image Processing: Algorithms and Systems II, SPIE Electronic Imaging*, San Jose, January 2003.

[19] P. M. Shankar, "A general statistical model for ultrasonic backscattering from tissues," *IEEE Trans. Ultrason. Ferroelect. Freq. Contr.*, vol. 47, pp. 727–736, Mar. 2000.

[20] A. M. Badawi, A. M. Hashem, A. S. Derbala, A. Hendawi, A. M. Youssef, M. F. Abdelwahab, "Ultrasonographic tissue signature for shistosomal liver and other related liver and other related liver pathologies", *In Proceedings of IEEE Ultrasonics, Ferroelectrics & Frequency Control Symposium* 1995.

[21] S. M. Emara, A. M. Badawi, Abou-Bakr M. Youssef, "Fuzzy Similarity Measures for Ultrasound Tissue Characterization ", *In Proceedings of Nonlinear Image Processing*, SPIE, 1995.

[22] Y. M. Kadah, Aly. A. Farag, Jacek M. Zurada, Ahmed M. Badawi, and Abou-Bakr M. Youssef, "Classification algorithms for quantitative tissue characterization of diffuse liver disease from ultrasound images," *IEEE Trans. Medical Imaging*, vol. 15, no. 4, pp. 466-478, August 1996.

[23] A. M. Badawi, Ahmed S. Derbala and Abou-Bakr M. Youssef, "Fuzzy logic algorithm for quantitative tissue characterization of diffuse liver diseases from ultrasound images," *International Journal of Medical Informatics* 55-2 pp. 135-147, 1999.

[24] A.N. Netravali and B.G. Haskell, *Digital pictures: representation, compression, and standards* (2nd Ed), Plenum Press, New York, NY (1995).

[25] D. Clausi and M.E. Jernigan, "A fast method to determine co-occurrence texture features," *IEEE Trans. Geosci. Remote Sensing*, vol. 36, pp. 298-300, Feb. 1998.

[26] D. Clausi and Y. Zhao, "An advanced computational method to determine co-occurrence probability texture features", *Geoscience and Remote Sensing Symposium*, 2002. IGARSS '02. 2002 IEEE International, vol. 4, pp. 2453 – 2455, 2002.

[27] J. Weickert, "Applications of nonlinear diffusion in image processing and computer vision",Acta Math. Univ. Comenianae, Vol. 70(1) (2001), pp. 33-50.

[28] G. Gilboa, Y.Y. Zeevi, N. Sochen," Image enhancement segmentation and denoising by time dependent nonlinear diffusion processes", *Proceedings. 2001 International Conference on Image Processing*, vol. 3, pp. 134 – 137, Oct. 2001.

[29] R. Touzi, "A review of speckle filtering in the context of estimation theory," *IEEE Trans. Geosci. Remote Sens.*, vol. 40, no. 11, pp. 2392–2404, Nov. 2002.

[30] J. Lee, "Digital image enhancement and noise filtering using local statistics," *IEEE Trans. Pattern Anal. Mach. Intell.*, vol. PAMI-2, no. 2, pp. 165–168, Mar. 1980.

[31] V. Frost, J. Stiles, K. Shanmugan, and J. Holzman, "A model for radar images and its application to adaptive digital filtering of multiplicative noise," *IEEE Trans. Pattern Anal. Mach. Intell.*, vol. PAMI-4, no. 2, pp. 157–166, Mar. 1982.

[32] D. T. Kuan, A. A. Sawchuk, T. C. Strand, and P. Chavel, "Adaptive noise smoothing filter for images with signal-dependent noise," *IEEE Trans. Pattern Anal. Mach. Intell.*, vol. PAMI-7, no. 2, pp. 165–177, Mar. 1985.

[33] D. T. Kuan, A. A. Sawchuk, T. C. Strand, and P. Chavel, "Adaptive restoration of images with speckle," *IEEE Trans. Acoust., Speech, Signal Process.*, vol. ASSP-35, no. 3, pp. 373–383, Mar. 1987.

[34] Y. Yu and T. Acton, "Speckle reducing anisotropic diffusion", *IEEE Trans. On Image Processing*, vol. 11, No. 11, pp. 1260-1270, November 2002.

[35] S. Aja-Fernandez and C. Alberola-lopez, "On the estimation of the coefficient of variation for anisotropic diffusion speckle filtering", *IEEE Trans. On Image Processing,* vol. 15, No. 9, pp. 2694-2701, September 2006.

[36] X. Hao, C. Bruce, C. Pislaru, and J. Greenleaf, "Identification of reperfused infracted myocardium from high frequency intracardiac ultrasound images using homodyned K distribution", *IEEE Ultrasonics Symposium*, pp. 1189-1192, 2001.

[37] X. Hao, C. Bruce, C. Pislaru, and J. Greenleaf, "Characterization of reperfused infracted myocardium from high-frequency intracardiac ultrasound images using homodyned K distribution", *IEEE Transaction on Ultrasonics, Ferroelectric, and Frequency Control*, vol. 49, no. 11, pp. 1530-1542, November 2002.

[38] R. Smolikova, M. Wachowiak, G. Tourassi, and J. Zurada "Neural estimation of scatterer density in ultrasound", *Proceedings of the 2002 International Joint Conference on Neural Networks*, vol. 2, pp. 1696 – 1701, 12-17 May 2002.

[39] M. Rabbani and P.W. Jones, *Digital image compression techniques*, vol. TT7, SPIE Optical Engineering Press, Bellvue, Washington (1991).

[40] Z. Yang and M. Fox, "Speckle reduction and structure enhancement by multichannel median boosted anisotropic diffusion", *EUROASIP Journal on Applied Signal Processing*, vol. 16, pp. 2492-2502, 2004.

[41] Z. Wang and A. C. Bovik, "A universal image quality index," *IEEE Signal Processing Letters*, vol. 9, no. 3, pp. 81–84, 2002.

[42] W. K. Pratt, *Digital Image Processing,* Wiley, New York, NY, USA, 1978.

[43] R.F. Wagner, M.F. Insana, "Analysis of ultrasound image texture via generalized Rician statistics," *Proc. SPIE* 556, pp. 153-159, 1985.

[44] P.M. Shankar, "A general statistical model for ultrasonic backscattering from tissues," *IEEE Trans. Ultrasonics Ferroelectrics and Freq. Control,* vol. 47, no. 3, pp. 727-736, 2000.

Ahmed Badawi (M'05-SM'06) received his BSC, MSC, PhD in 1990, 1993, and 1996 respectively from Department of Systems & Biomedical Engineering, Cairo University.

He was an assistant professor, associate professor, and full professor in 1996, 2001, and 2007 respectively at Systems & Biomedical Engineering Cairo University. He is a visiting professor at University of Tennessee, Biomedical Engineering Department since August 2005. He is a professor on leave at Systems & Biomedical Engineering, Cairo University. His research interests are in Medical Imaging, 3D/4D Ultrasound Scanning, Reconstruction, Visualization, and Measurements, 4D Surgical Navigation, Image Processing, Computer Vision and Pattern Recognition in Medicine, Neural Networks, Fuzzy Systems, Medical Classification, Biometrics, Intelligent Medical Systems, Medical Software Workstations. He is a reviewer of several international journals, chairman of several international conferences sessions and track chairman.

Dr. Badawi is a senior member, IEEE, a member in IEEE Engineering in Medicine and Biology society. Dr. Badawi published over 75 papers in journals and peer reviewed conferences. He awarded several prestigious awards such as Egyptian National Academy for Scientific Research and Technology, Cairo University award for Engineering Research. Dr. Badawi was a director of Imaging Solutions Department at ibetech.com where he was the head of the team who developed the first 3D ultrasound system in Egypt.

Dr. Badawi has over 17 years experience in Systems & Biomedical Engineering teaching and research. Dr. Badawi supervised over 15 MSc and 2 PhD students.
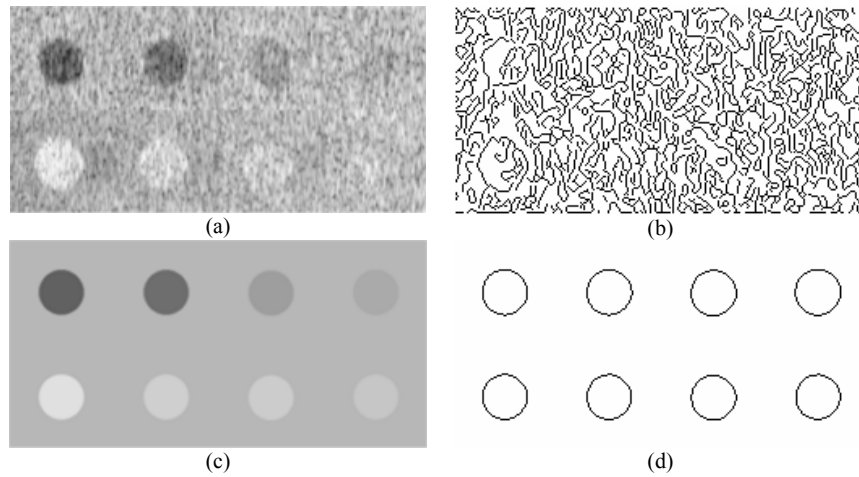
Fig. 1 Contrast detail phantom of resolution 256x128 (a), and its Canny edge map (b), Reference contrast detail phantom (c), and its Canny edge map (d)
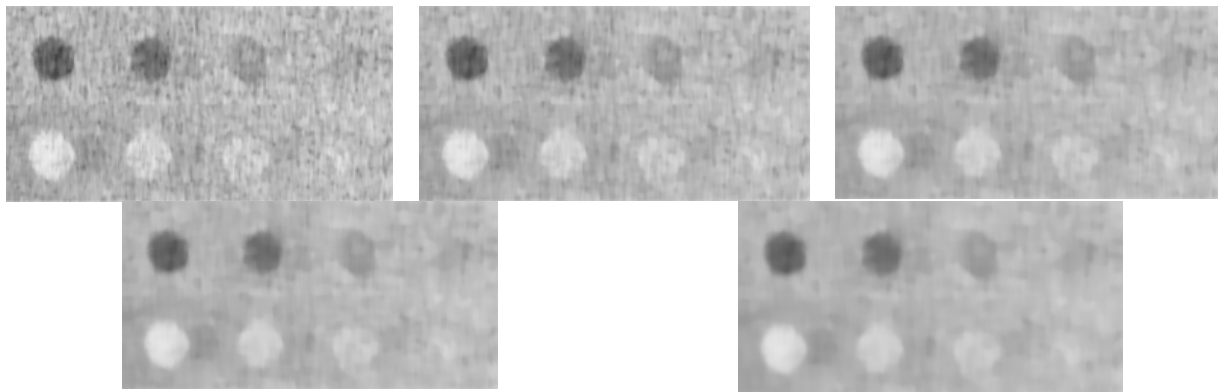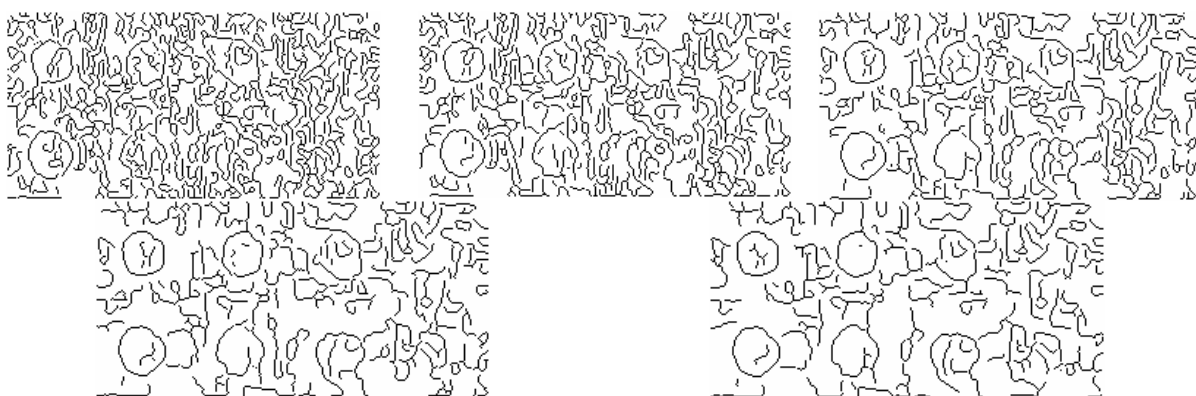

Fig. 2 Diffused images at iterations 1, 2, 3, 4, and 5
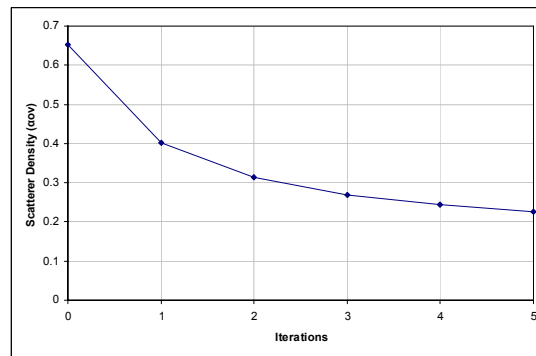

Fig. 3 Canny edge maps at iterations 1, 2, 3, 4, and 5

Fig. 4 Time evolution of the α_{ov} of the phantom image through diffusion using (29)
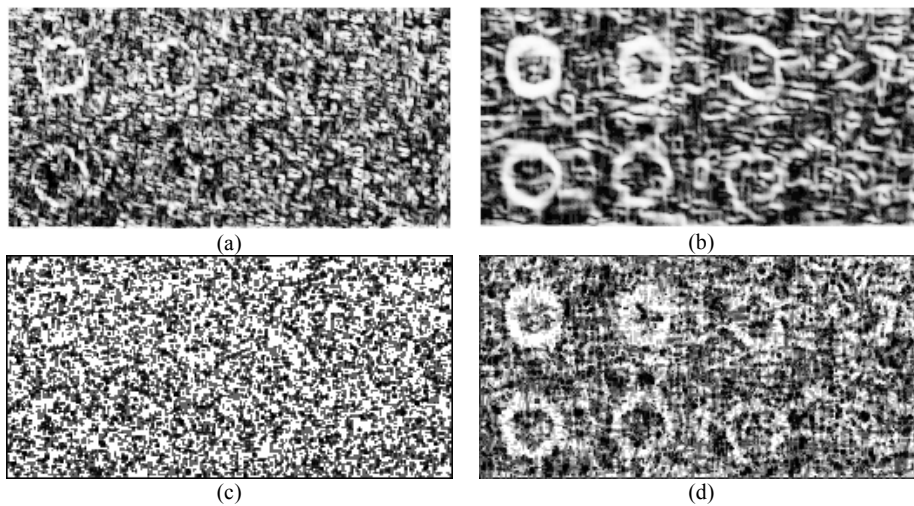
Fig. 5 Normalized Gradient (a,b) and Scatterer density (c,d) maps at iteration 1 and 5
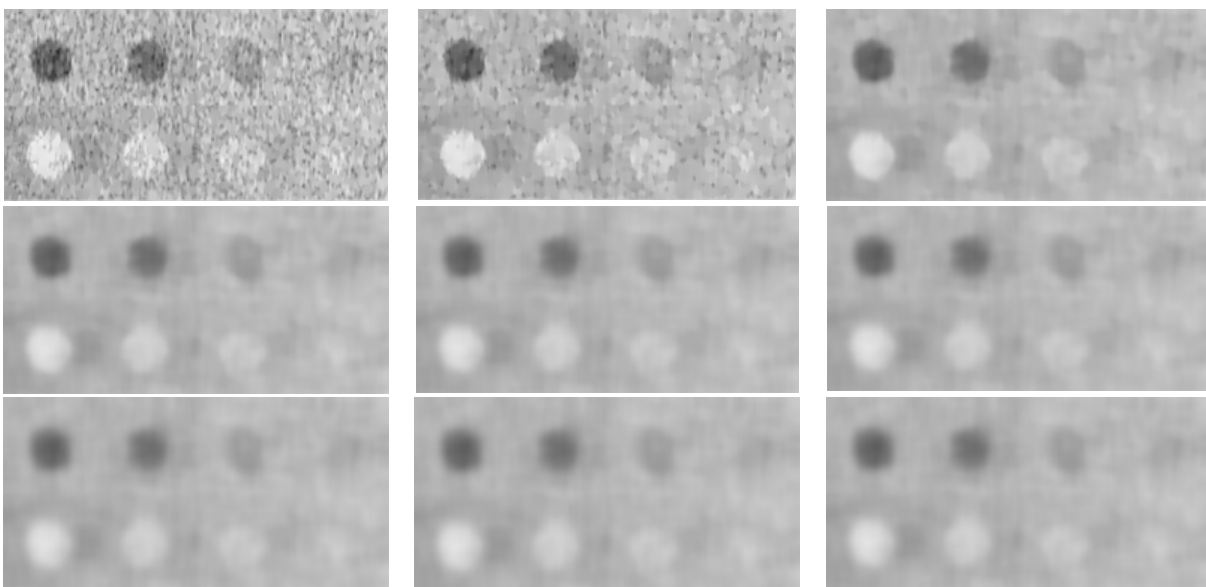
Fig. 6 Diffused images for K=0.01, 0.1, 0.5, 1, 1.5, 2, 10, 100, and 1000
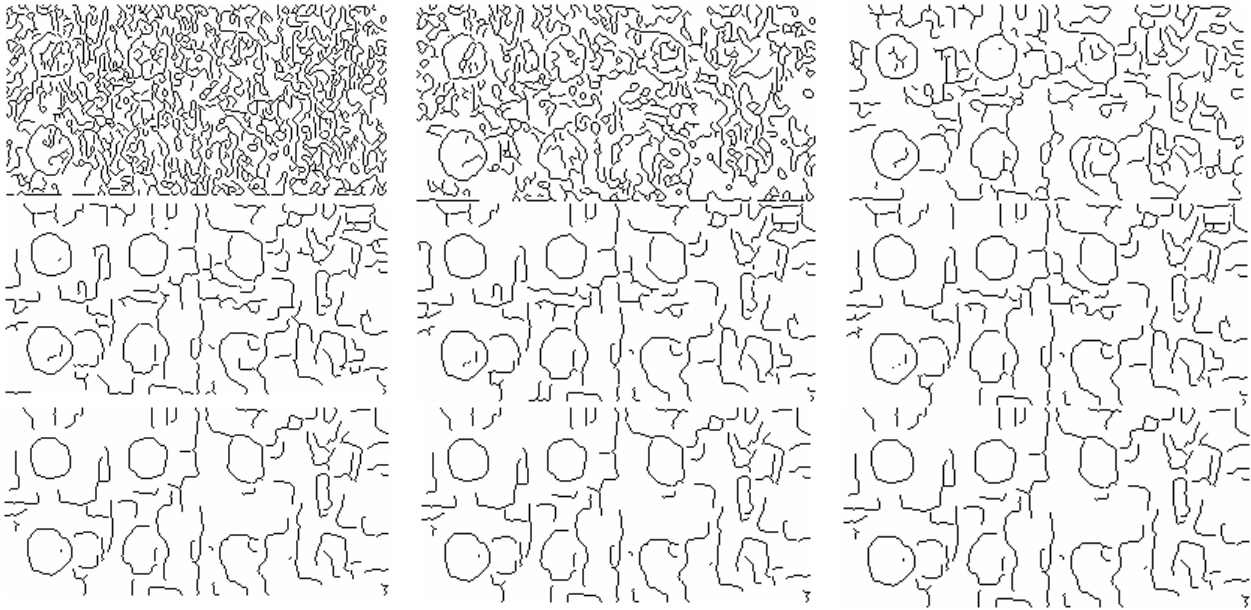
Fig. 7 Canny edge maps for diffused images for K=0.01, 0.1, 0.5, 1, 1.5, 2, 10, 100, and 1000

(a)

(b)

(c)

(d)
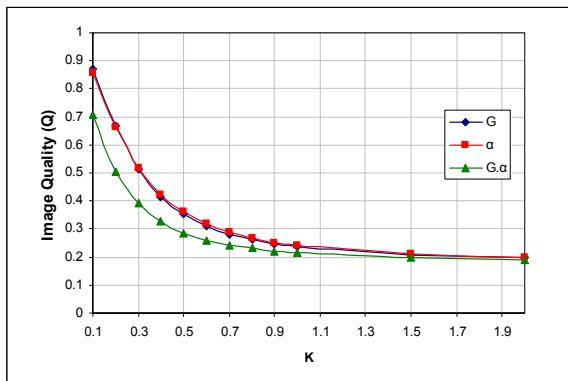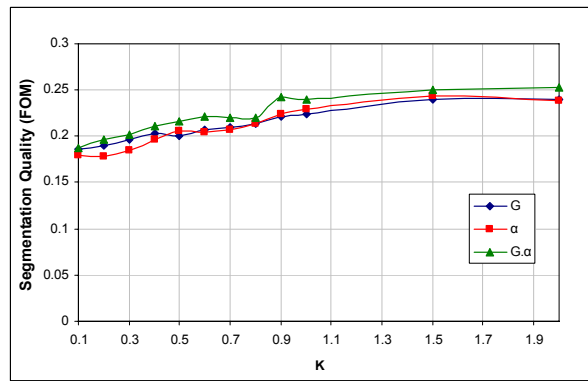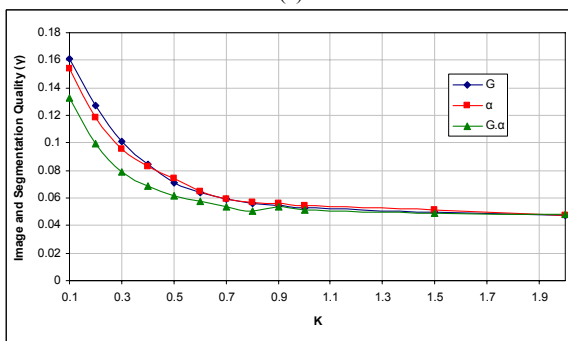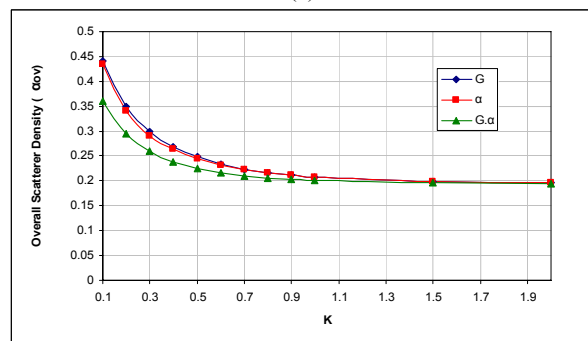
Fig. 8 Q (a), FOM (b), γ (c), and α_{ov} (d) plots versus Conductance K for the three diffusivity functions in (36-38)
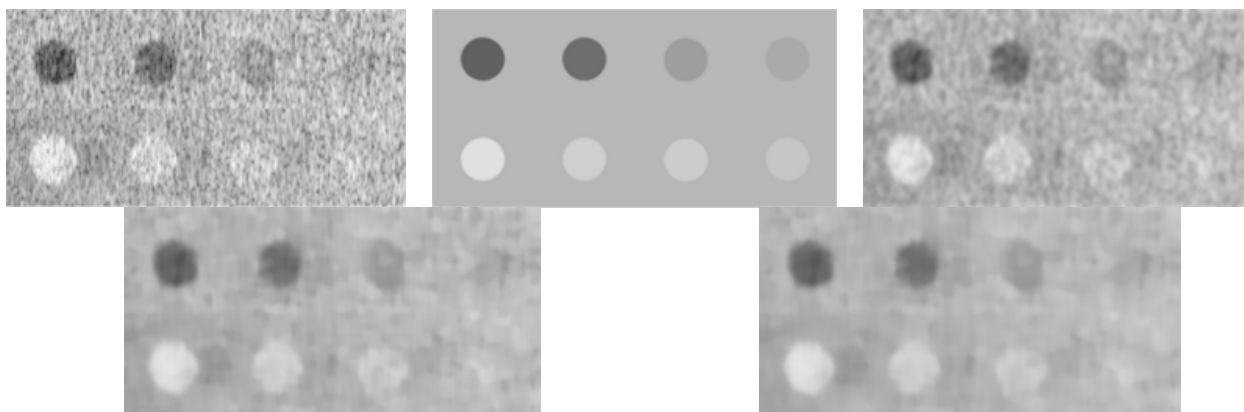
Fig. 9 Original phantom image (a), reference image (b), diffused image using Gaussian with σ=1 (c), gradient weighted nonlinear diffusion (d), and using our diffusivity function (e) weighted by (31)
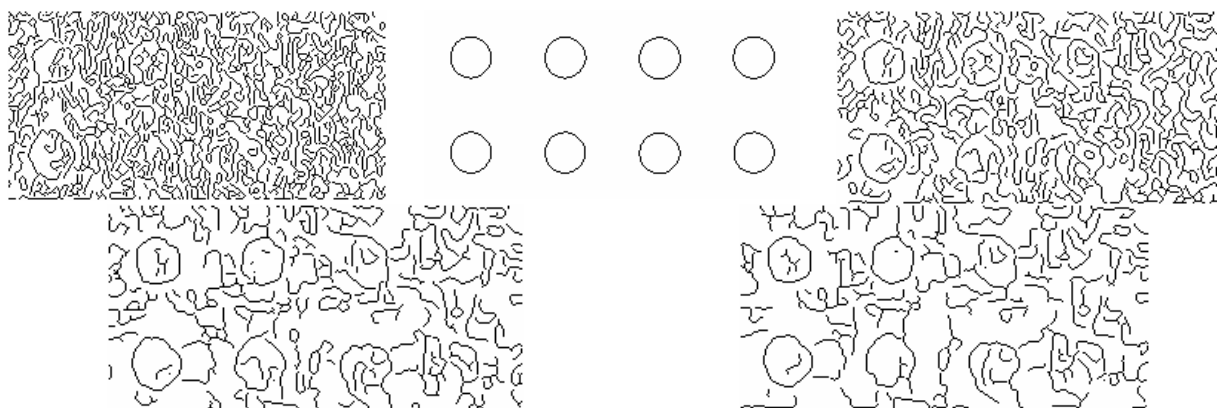
Fig. 10 Canny edge maps for Fig. 9

(a)

(b)

(c)

(d)
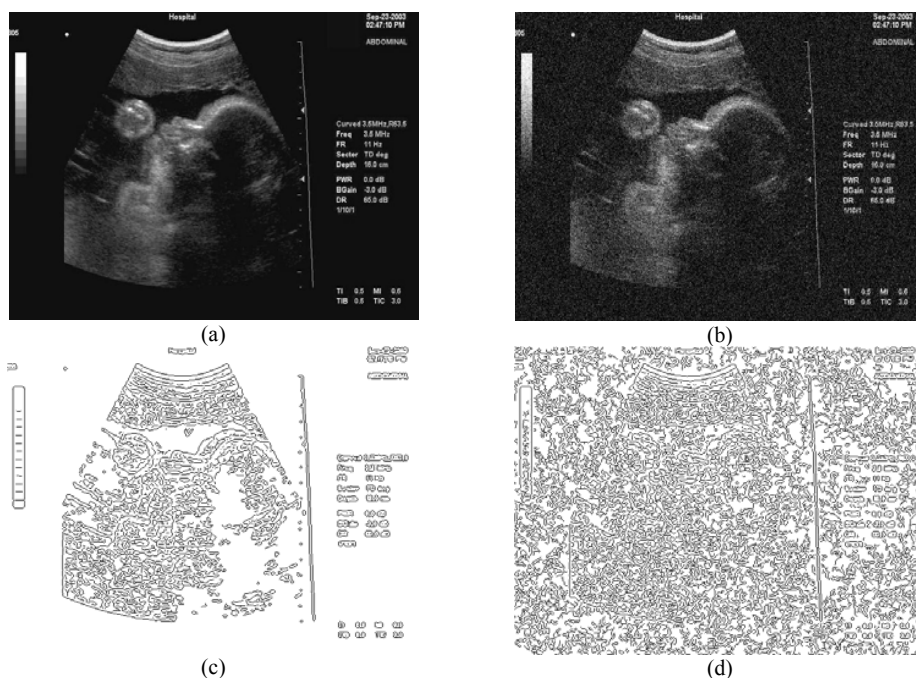
Fig. 11 Fetal face original image (a), corresponding image with additive Gaussian noise of standard deviation of 20 (b), original Canny edge map (c), Gaussian noisy Canny edge map (d)
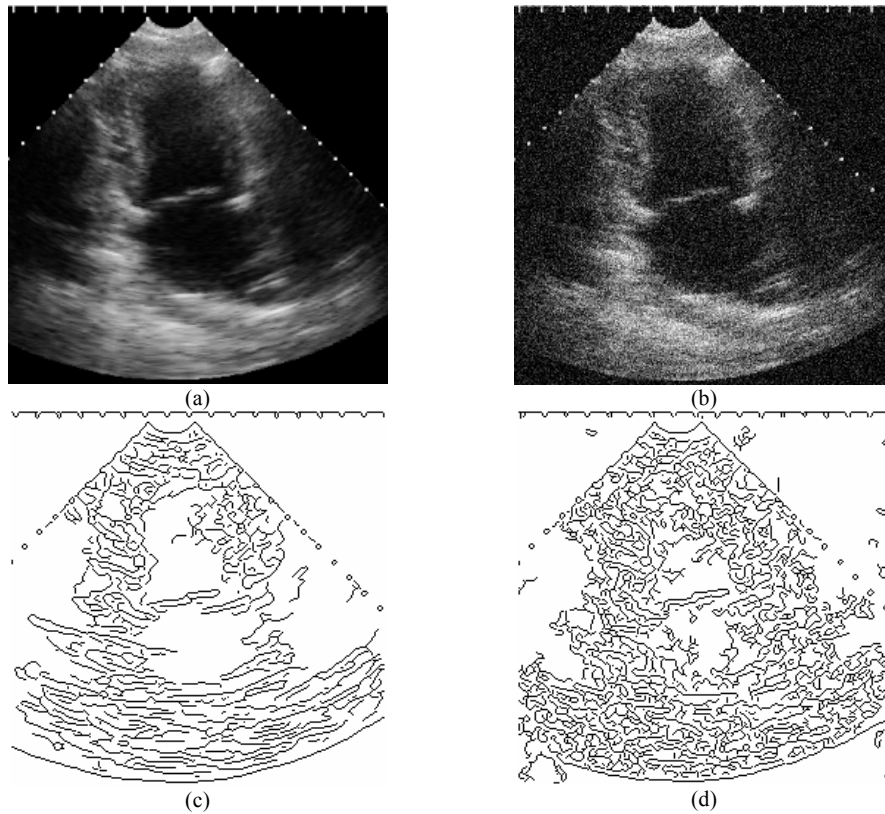
Fig. 12 Heart original image (a), its corresponding image with additive Gaussian noise of standard deviation of 20 (b), original Canny edge map (c), Gaussian noisy Canny edge map (d)
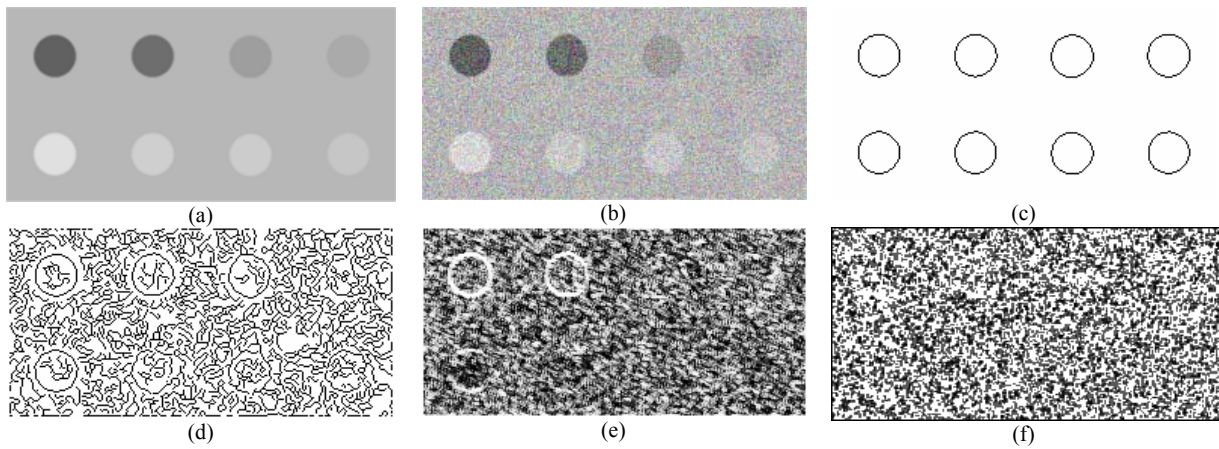
Fig. 13 Phantom reference original image (a), its corresponding image with additive Gaussian noise of standard deviation of 20 (b), riginal reference Canny edge map (c), Gaussian noisy Canny edge map (d), normalized noisy gradient map (e), normalized noisy scatterer density map (f)
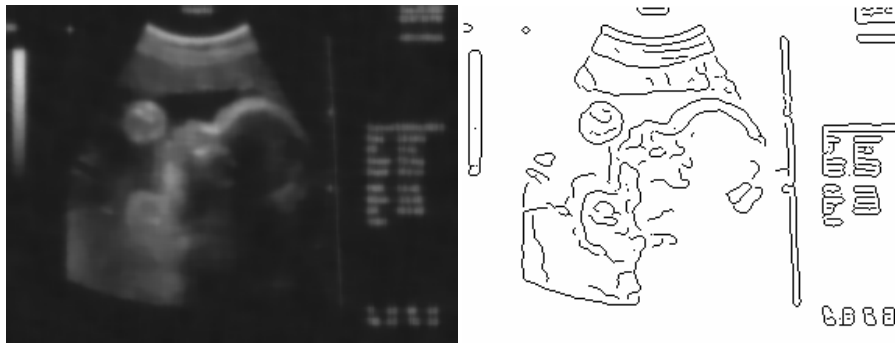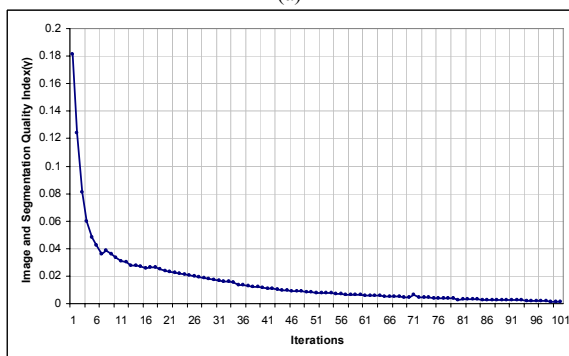
Fig. 14 Diffused fetal face image and its Canny edge map
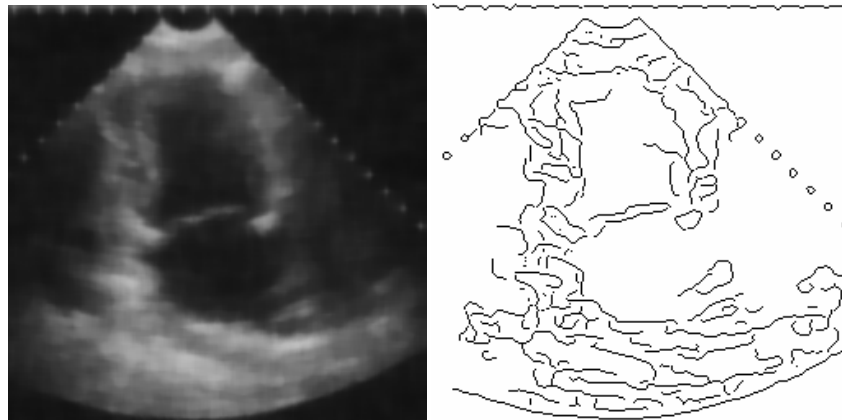
Fig. 15 Diffused heart image and its Canny edge map

(a)

(b)

(c)

(d)
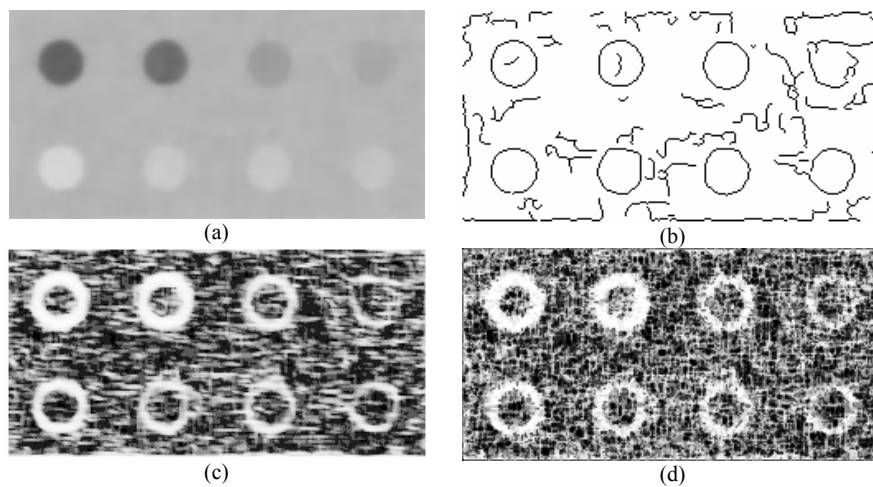
Fig. 16 Diffused noisy phantom reference image (a), its Canny edge map (b), its normalized gradient map (d), and normalized its scatterer density map (e)
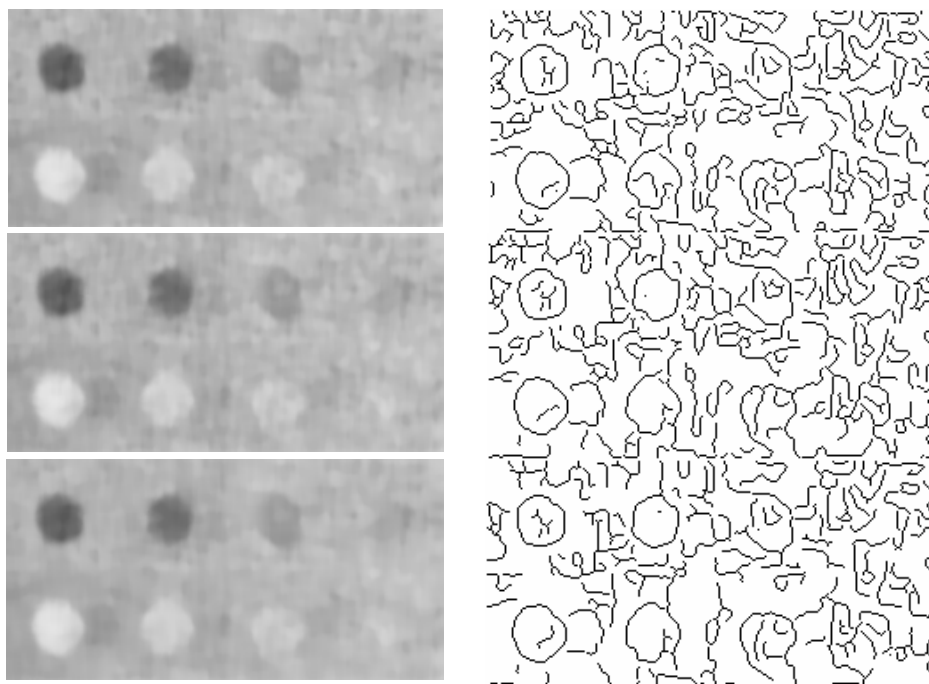
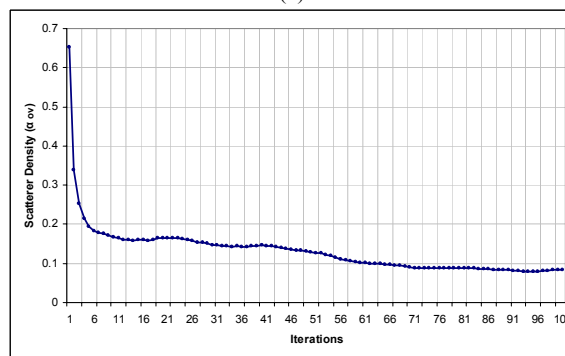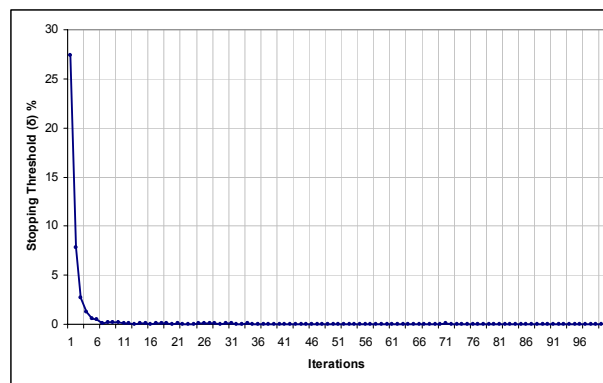Fig. 17 Diffused images using the three diffusivity functions in equations (36-38)
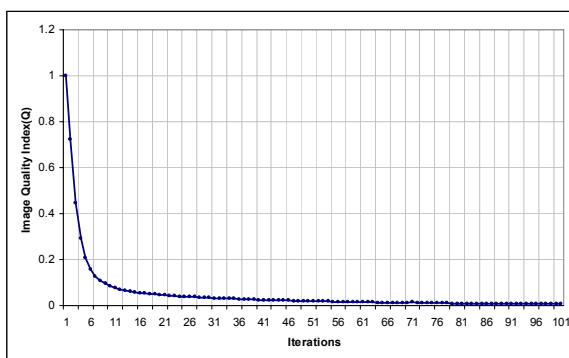
(a)
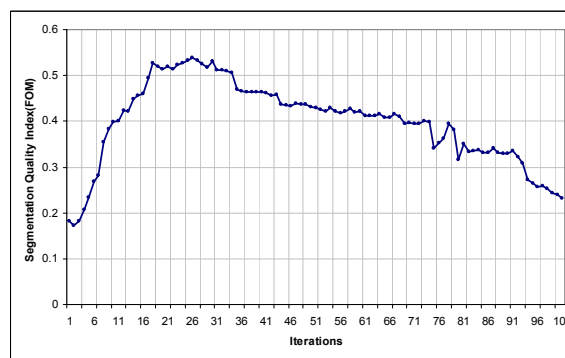
(b)

(c)

(d)

(e)

Fig. 18 Time evolution of the Q (a), FOM (b), γ (c), α_{ov} (d), and δ (e) of the nonlinear diffusion for 100 iterations

Fig. 19 Diffused image and its Canny edge map at iteration 3 for the stopping criteria of δ<3%
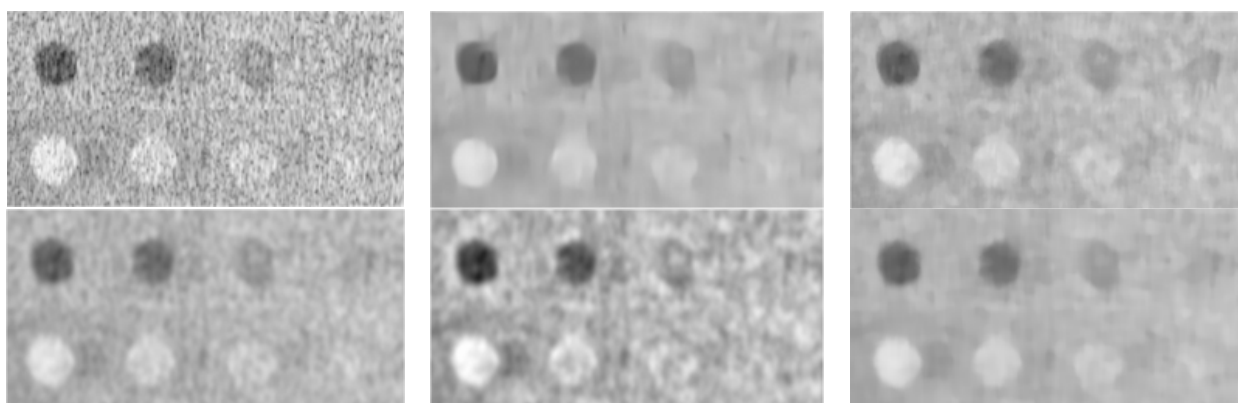

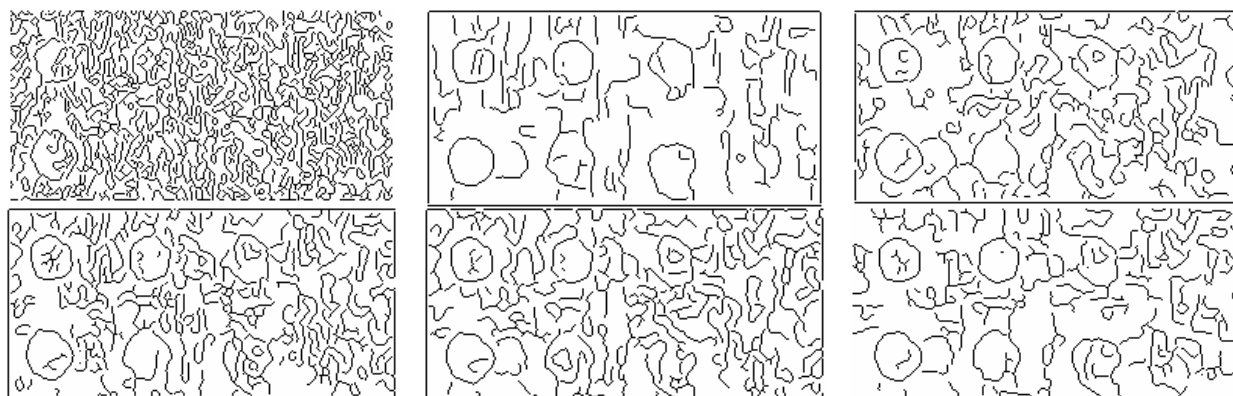Fig. 20 Original image, processed images with NCD, AWFM, WS, WSCE, and SDWNAD

Fig. 21 Canny edge maps for original phantom, NCD, AWFM, WS, WSCE, and SDWNAD